Available online at www.sciencedirect.com
ScienceDirect
Journal of Power Sources 174 (2007) 246–254
JOURNAL OF POWER SOURCES
www.elsevier.com/locate/jpowsour

Comparison of different current collecting modes of anode supported micro-tubular SOFC through mathematical modeling

Daan Cui [a,b], Lin Liu [a], Yonglai Dong [a], Mojie Cheng [a,*]

[a] *Dalian Institute of Chemical Physics, Chinese Academy of Sciences, 457 Zhongshan Road, Dalian 116023, PR China*
[b] *Graduate School of the Chinese Academy of Sciences, Beijing 100049, PR China*

Received 6 July 2007; received in revised form 18 August 2007; accepted 30 August 2007
Available online 4 September 2007

Abstract

A two-dimensional model comprising fuel channel, anode, cathode and electrolyte layers for anode-supported micro-tubular solid oxide fuel cell (SOFC), in which momentum, mass and charge transport are considered, has been developed. By using the model, tubular cells operating under three different modes of current collection, including inlet current collector (IC), outlet current collector (OC) and both inlet and outlet collector (BC), are proposed and simulated. The transport phenomena inside the cell, including gas flow behavior, species concentration, overpotential, current density and current path, are analyzed and discussed. The results depict that the model can well simulate the diagonal current path in the anode. The current collecting efficiency as a function of tube length is obtained. Among the three proposed modes, the BC mode is the most effective mode for a micro-tubular SOFC, and the IC mode generates the largest current density variation at *z*-direction.
© 2007 Elsevier B.V. All rights reserved.

Keywords: Solid oxide fuel cells; Micro-tube; Modeling; Current collection

1. Introduction

Solid oxide fuel cells (SOFCs) are one of the most promising power generation technologies because of their high efficiency and clean generation of electric power [1,2]. Tubular SOFCs have several advantages compared with planar ones. For example, the sealing area is much smaller in a tubular cell than in a planar cell [3]. Fuel and air distribution manifolds can be more facile in tubular stacks. Thermal stresses can be less troubled in tubular systems because each membrane-electrode assembly is less rigidly restricted. Recent years, anode supported tubular SOFC has been rapidly developed [4–8]. The much longer current path in a tubular SOFC than in a planar cell becomes one of the most concerned issues. Especially for an anode supported micro-tubular SOFC, current at the anode side can only be drawn from anode ends. The current collecting mode is very important in tubular cells for achieving high cell efficiency.

Numerical calculations are a very useful tool in the SOFC research because the detailed measurement on the phenomena in SOFCs is difficult [9–11]. Up to now, most cell performance simulations have been carried out using the circuits of an equivalent circuit of a cell portion plus a resistance portion, namely, a ladder circuit [10–12]. The current-flow directions obtained from these models are inconsistent with the facts in a real cell. When there is a large difference of the electromotive force (EMF) and a long current path in a cell, the current may flow diagonally in the electrolyte and electrodes, and the ladder equivalent circuit model cannot simulate the diagonal current in the electrolyte and electrodes precisely [12]. In order to deal with the diagonal current in the electrolyte and electrodes, it is necessary to develop a new model for simulating the current path in the cell components.

In this paper, a two-dimensional model comprising fuel channel, anode, cathode and electrolyte layers for anode-supported micro-tubular solid oxide fuel cell will be built. The calculations of electro-chemical, fluid phenomena and current path inside the single tubular cell are correlated to each other. We will investigate the current density at the anode/electrolyte interface and the current collecting efficiency under three different current collecting modes of inlet current collector (IC),

Abbreviations: BC, both inlet and outlet collector; EMF, electromotive force; IC, inlet current collector; OC, outlet current collector; SOFC, solid oxide fuel cell; TC, total area current collector

* Corresponding author. Tel.: +86 411 84379049; fax: +86 411 84379049.
E-mail address: mjcheng@dicp.ac.cn (M. Cheng).

0378-7753/$ – see front matter © 2007 Elsevier B.V. All rights reserved.
doi:10.1016/j.jpowsour.2007.08.094

Nomenclature

c	concentration (mol m^{-3})
D	diffusion coefficient (m^2 s^{-1})
E_0	standard potential (V)
F	Faraday's constant (96485 C mol^{-1})
i	current density (A m^{-2})
i_0	exchange current density (A m^{-2})
I	current (A)
K	permeability (m^2)
n_e	electron transferred per reacting
p	pressure (atm)
R_g	gas constant (J mol^{-1} K^{-1})
T	temperature (K)
u	velocity (m s^{-1})
V_{cell}	cell voltage (V)

Greek letters

β	transfer coefficient
ε	porosity
ϕ	potential (V)
η	overpotential (V)
μ	dynamic viscosity (m^2 s^{-1})
ρ	density (kg m^{-3})
σ	conductivity (S m^{-1})
τ	tortuosity factor

Subscripts

a	anode
act	activation
c	cathode
diff	diffusion
ele	electrolyte
K	Knudsen diffusion
m	ordinary diffusion
rev	reversible
0	standard

outlet current collector (OC) and both inlet and outlet collector (BC).

2. Model description

2.1. Basic feature of the cell and model geometry

For a micro-tubular cell, current collector at anode side is only attached to the end of the anode tube. H_2 humidified at room temperature is introduced as a fuel at the flow rate of 30 cm^3 min^{-1}. Oxygen concentration at the cathode/air interface is assumed to be the same as in air. Using this model, the cell performances with different tube length are calculated. The effects of three different current collecting modes are analyzed. The dimensions of the cell are listed in Table 1.

The anode supported tubular cell consists of YSZ electrolyte, Ni-YSZ anode and LSM-YSZ cathode. Because the micro-tubular cell has a symmetrical structure, it is assumed that the cell properties are uniform in each angular section. Thus, one geometrical dimension is neglected, and the 2D modeling is considered for the entire cell performance, as shown in Fig. 1. The current collector at the anode side is attached to one or two tube ends, whereas the current collector at the cathode side was connected to the whole cathode. The anode tube length and current collecting modes are crucial for the reduction of efficiency loss [8].

Table 1
Input parameters to model [12,22]

Anode conductivity (S m^{-1})	$\sigma_a = \frac{95\times10^6}{T} \times \exp\left(\frac{-1150}{T}\right)$
Cathode conductivity (S m^{-1})	$\sigma_c = \frac{42\times10^6}{T} \times \exp\left(\frac{-1200}{T}\right)$
Electrolyte conductivity (S m^{-1})	$\sigma_e = 3.34\times10^4 \times \exp\left(\frac{-10300}{T}\right)$
Tubular interior diameter (mm)	1.49
Anode thickness (mm)	0.72
Cathode thickness (μm)	50
Electrolyte thickness (μm)	50
Transfer coefficient (β)	0.5
Electron transferred per reacting (n_e)	1
Anode exchange current density ($i_{0,a}$) (A m^{-2})	5300
Cathode exchange current density ($i_{0,c}$) (A m^{-2})	2000
K (m^2)	1e−12
μ_{H_2} (Pa s)	21.63e−7
μ_{H_2O} (Pa s)	40.45e−7
$D_{O_2,c}$ (m^2 s^{-1})	7.588e−6
$D_{N_2,c}$ (m^2 s^{-1})	7.588e−6
$D_{channel,m}$ (m^2 s^{-1})	8.506e−4
$D_{H_2,a}$ (m^2 s^{-1})	3.14e−5
$D_{H_2O,a}$ (m^2 s^{-1})	1.39e−5

Three modes of current collection, including inlet current collector (IC), outlet current collector (OC), both inlet and outlet collector (BC) are proposed and calculated. In order to compare current collecting efficiency under the three different current collecting modes, the cell performance with all anode interior surfaces for current collection (TC) was also calculated as a reference. The current-collecting efficiency is defined as the cell

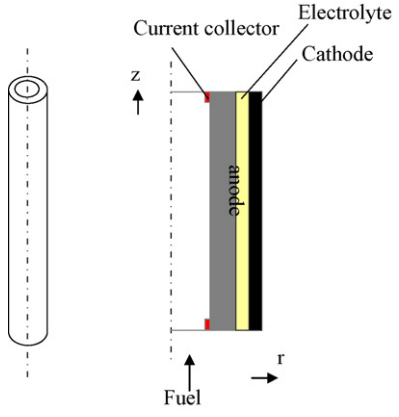

Fig. 1. Schematic diagram of a micro-tubular geometry in 2D.

performance ratio of the proposed current collecting mode to the TC mode.

2.2. Model assumptions

- The model is based on steady state, using humidified H_2 as the fuel.
- Gas flows in the channels are laminar.
- The reactant gas mixtures are approximated as ideal gas and incompressible. The fuel cell operates with 100% current efficiency.
- The model is assumed to be isothermal, and the cell run at 800 °C.

2.3. Electrochemical model

The reactions to deal with the SOFC model are those commonly reported in the literature [13,14]. The oxygen anions from oxygen reduction at cathode pass through the electrolyte and react with hydrogen at the anode–electrolyte interface:

$$\tfrac{1}{2}O_2 + 2e^- \rightarrow O^{2-} \tag{1}$$

$$H_2 + O^{2-} \rightarrow H_2O + 2e^-. \tag{2}$$

Activation polarization losses occur from slow electron release or capture steps at the electrode–electrolyte interfaces. The Butler–Volmer kinetic equations are generally adopted for expressing the local current density distribution [15].

$$i_a = i_{a,0}\left\{\exp\left(\beta\frac{n_e F\eta_{Act}}{R_g T}\right) - \exp\left[-(1-\beta)\frac{n_e F\eta_{Act}}{R_g T}\right]\right\} \tag{3a}$$

$$i_c = i_{c,0}\left\{\exp\left(\beta\frac{n_e F\eta_{act}}{R_g T}\right) - \exp\left[-(1-\beta)\frac{n_e F\eta_{act}}{R_g T}\right]\right\} \tag{3b}$$

$i_{a,0}$ is 5300 A m^{-2} for a Ni-YSZ anode, $i_{c,0}$ is 2000 A m^{-2} for a LSM-YSZ cathode. The activation loss can be calculated according to the following equation:

$$\eta_{act} = \phi_{rev} - |\phi_{electrode} - \phi_{ele}| \tag{4}$$

where ϕ_{rev} is the reversible potential between the electrode and the electrolyte. ϕ_{rev} can be obtained from Nernst equation. Since the electrochemical active layer is usually very thin compared with the electrode, the current generation is considered to take place only at the electrode–electrolyte interfaces [14].

In expression (3a), $i_{a,0}$, $i_{c,0}$ and β are the exchange current density and the transfer coefficient (A m^{-2}). The transfer coefficient is considered to be the fraction of the change in polarization that results in a change in the reaction rate constant. The exchange current density is the forward and reverse electrode reaction rate at the equilibrium potential, and a high exchange current density means that a high electrochemical reaction rate and good fuel cell performance can be expected [16].

Electronic charge at the anode:

$$-\nabla(\sigma_a \nabla\phi_a) = 0 \tag{5a}$$

anode/electrolyte interface boundary:

$$-\sigma_a \nabla\phi_a \cdot n = -i_a \tag{5b}$$

anode current collector boundary:

$$\phi_{anode} = 0 \tag{5c}$$

other anode boundaries:

$$-\sigma_a \nabla\phi_a \cdot n = 0 \tag{5d}$$

Ionic charge at the electrolyte:

$$-\nabla(\sigma_{ele} \nabla\phi_{ele}) = 0 \tag{6a}$$

anode/electrolyte interface boundary:

$$-\sigma_{ele} \nabla\phi_{ele} \cdot n = i_a \tag{6b}$$

cathode/electrolyte interface boundary:

$$-\sigma_{ele} \nabla\phi_{ele} \cdot n = -i_c \tag{6c}$$

other electrolyte boundaries:

$$-\sigma_{ele} \nabla\phi_{ele} \cdot n = 0 \tag{6d}$$

Electronic charge at the cathode:

$$-\nabla(\sigma_c \nabla\phi_c) = 0 \tag{7a}$$

cathode/electrolyte interface boundary:

$$-\sigma_c \nabla\phi_c \cdot n = i_c \tag{7b}$$

cathode current collector boundary:

$$\phi_c = V_{cell} \tag{7c}$$

other cathode boundaries:

$$-\sigma_c \nabla\phi_c \cdot n = 0. \tag{7d}$$

2.4. Momentum and mass transport equations

To calculate the velocity distribution in the gas channel, the steady-state incompressible Navier–Stokes equation, Eq. (8a) and Eq. (8b) are solved numerically [17]:

$$\rho(u\nabla u) - \nabla\mu(\nabla u + (\nabla u)T) + \nabla P = 0 \tag{8a}$$

$$\nabla u = 0 \tag{8b}$$

The inlet fuel is composed of H_2O and H_2 (0.97:0.03 in molar fractions), flowing at a volume velocity of 30 sccm at room temperature. The density (ρ) is calculated from the ideal gas law, and the mean molar dynamic viscosity (μ) is obtained from the product of individual viscosity and molar fraction. An initial gas volume velocity of 30 sccm and a pressure (P_0) of 101325 Pa are applied to the gas inlet and outlet boundaries Eqs. (8c) and (8d).

At the interfaces of electrolyte and electrode, no slip conditions are employed Eq. (8e).

$$u \cdot n = u_0 \tag{8c}$$

$$n(-\nabla\mu(\nabla u + (\nabla u)T) + \nabla P) = -nP_0 \tag{8d}$$

$$u = 0 \tag{8e}$$

Darcy equation describes the flow in the porous structure well far away from the walls, but it cannot model a no-slip condition near a wall. Thus, Brinkman equation is used for the porous media [18,19].

$$\nabla P = \mu\nabla^2 u + \frac{\mu}{K}u \tag{9}$$

where K is the permeability of the medium considered.

Mass diffusion coefficients are required whenever species transport equations in multi-component flows are solved. Diffusion in porous medium is usually described by molecular diffusion or Knudsen diffusion. Knudsen diffusion occurs when the pore diameter is smaller than the mean free path of the gas molecules. Molecular diffusion occurs when the pore diameter is larger than the mean free path of the gas molecules. For an SOFC, both Knudsen and ordinary molecular diffusion process have to be considered [20]. The overall effective diffusion coefficient is given by [15]

$$D_i = \frac{\varepsilon}{\tau}\left(\frac{1}{D_{i,\mathrm{m}}} + \frac{1}{D_{\mathrm{K}}}\right)^{-1} \tag{10}$$

where ε, τ, $D_{i,\mathrm{m}}$ and D_{k} denotes porosity of porous medium, tortuosity factor, the ordinary and Knudsen diffusion coefficients[21], respectively. Finally, the steady-state diffusion and convection equation of Eq. (11) is solved from the velocity distribution to obtain the concentration distribution of reactants and products in the gas channel and the electrodes.

$$\nabla(-D_i\nabla c_i + c_i u) = 0 \tag{11}$$

anode/electrolyte interface boundary:

$$(-D_{\mathrm{H_2,a}}\nabla c_{\mathrm{H_2}} + c_{\mathrm{H_2}}u)\cdot n = -\frac{i_{\mathrm{a}}}{2F} \tag{12a}$$

$$(-D_{\mathrm{H_2,a}}\nabla c_{\mathrm{H_2O}} + c_{\mathrm{H_2O}}u)\cdot n = \frac{i_{\mathrm{a}}}{2F} \tag{12b}$$

anode channel inlet:

$$c_{\mathrm{H_2}} = c_{\mathrm{H_2},0} \tag{12c}$$

$$c_{\mathrm{H_2O}} = c_{\mathrm{H_2O},0} \tag{12d}$$

anode channel outlet:

$$(-D_{\mathrm{channel,m}}\nabla c_i + c_i u)\cdot n = c_i u \cdot n \tag{12e}$$

cathode/electrolyte interface boundary:

$$(-D_{\mathrm{O_2,c}}\nabla c_{\mathrm{O_2}} + c_{\mathrm{O_2}}u)\cdot n = -\frac{i_{\mathrm{c}}}{4F} \tag{13a}$$

O_2 concentration at the cathode/air interface is equal to the O_2 concentration in air as assumed at Section 2.1.

$$c_{\mathrm{O_2}} = c_{\mathrm{O_2},0} \tag{13b}$$

other boundaries:

$$(-D_i\nabla c_i + c_i u)\cdot n = 0. \tag{13c}$$

2.5. Numerical implementation

The calculations are solved using the finite element commercial software COMSOL MULTIPHSICS®, Version 3.3a. Because the primary objective in this modeling is to compare the cell performance under the different current collecting modes and the current density distribution, the mathematical simulation was performed at 0.7 V. The outputs from the model are the distributions of velocity, current density and species concentrations.

3. Results and discussion

3.1. Flow behavior and distribution of species

From the simulation, it is evident that velocity decreases rapidly in the porous anode. Fig. 2 shows the calculated profile of the velocity for the fuel flow in the channel and the anode. Because the constant temperature and the incompressible gases are assumed, the velocity profile changes slightly along the z-direction. The velocity close to fuel channel wall is obviously falling due to the viscosity stress. In this simulation, the mixed gases of H_2/H_2O with a channel center velocity of about 2 m s^{-1}

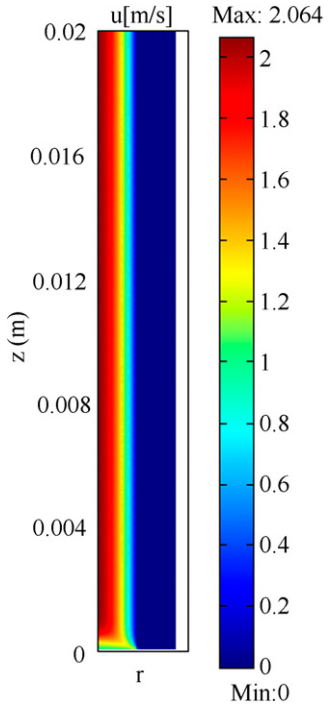

Fig. 2. Surface plot of velocity profile for fuel in anode and fuel channel for a 2 cm long SOFC (current collector at inlet).

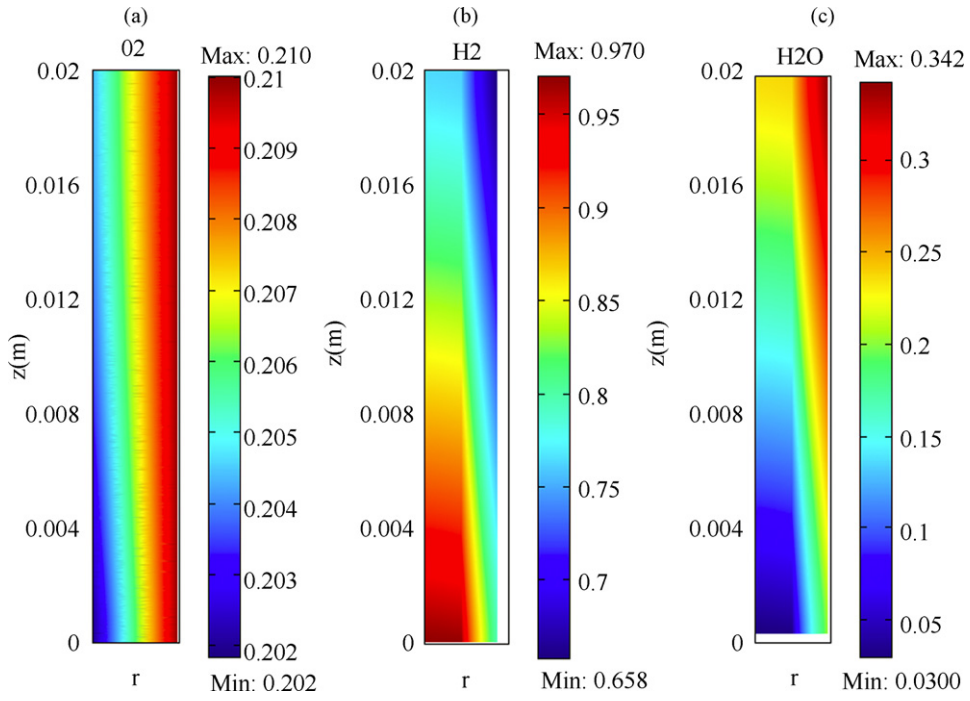

Fig. 3. Surface plots of O_2 (a), H_2 (b) and H_2O (c) and molar fraction distribution for a 2 cm long SOFC (only current collector at inlet).

are imported from the SOFC fuel channel inlet at 800 °C. The velocity of fuel flow in anode is reduced to about 10^{-6} of that in the channel.

Fig. 3(a) shows the distribution of oxygen molar fraction in the porous cathode. Due to the oxygen reduction reaction, the oxygen molar fraction decreases from the cathode/air interface to cathode/electrolyte interface. The distributions of hydrogen and water vapor molar fractions in the anode channel and porous anode are shown in Fig. 3(b) and (c). Since the hydrogen consumption occurs at the anode/electrolyte interface, the hydrogen molar fraction decreases along the fuel-flow direction, whereas the water vapor molar fraction increases along the *z*-direction. The variations of hydrogen and water vapor molar fractions in the porous anode along *r*-direction are very sharp but very slow in fuel channel. These results show that species transport resistance of porous anode can lower the fuel gas diffusion velocity in porous anode and reduce the cell performance. In one word, the overall cell performance of anode-supported tubular SOFC can be limited by the fuel gas diffusion velocity in the thick porous anode.

Fig. 4 shows the variation of H_2 molar fraction along the anode/electrolyte interface. H_2 molar fraction decreases along the fuel-flow direction under all the four current collecting modes. The H_2 molar fraction at inlet is smaller under the IC mode than under the OC mode. The variation of H_2 molar fraction along the *z*-direction is the mildest under the IC mode. Thus, the electrochemical reaction at fuel inlet is faster under the IC mode than under the OC mode. It is also shown in Fig. 4 that the reaction at the outlet is relatively slow under the IC mode, and H_2 molar fraction at outlet is the highest among four current-collecting modes. The variation of H_2 molar fraction is much sharper under the OC mode than under the IC mode. The main reason is that the inlet electrochemical reaction is milder under the OC mode than under the other modes, and less H_2 is consumed. However, the reaction at outlet is relatively faster under the OC mode than under the other modes, and more H_2 is consumed at outlet. The H_2 molar fractions under both the BC and TC modes are the same as that under the IC mode at inlet, and decreases from inlet to outlet with a rate similar to that under the OC mode, indicating a higher H_2 depleting rate under the two modes. It can be seen in Fig. 4 that the variation of H_2O molar fraction along the anode/electrolyte interface is opposite to that of H_2.

Fig. 5 shows the changes of O_2 molar fraction along the cathode/electrolyte interface. Since O_2 molar fraction at the cathode/air interface is assumed to be equal to that in the air (0.21), the amount of O_2 consumed in electrode can obviously

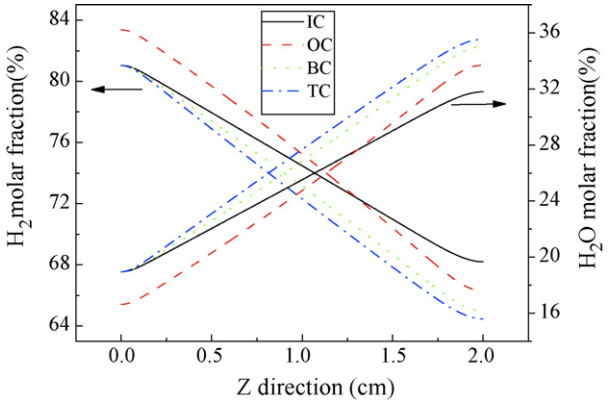

Fig. 4. H_2 and H_2O molar fractions along the anode/electrolyte interface for a 2 cm long SOFC.

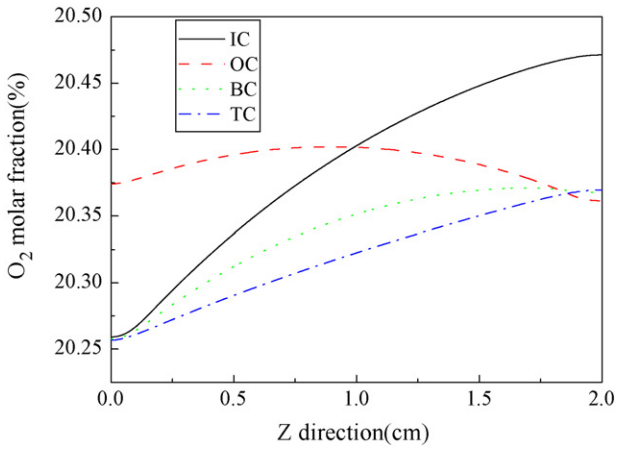

Fig. 5. O_2 molar fraction along the cathode/electrolyte interface for a 2 cm long SOFC.

be seen. Under the IC, BC and TC modes, the consumed O_2 fractions at the inlet are very close and higher than that under the OC mode, and the O_2 molar fraction at electrolyte/cathode interfaces increases from inlet to outlet. However, O_2 molar fraction exhibits a parabola-like curve under the OC mode, indicating that the O_2 consumption is quite even along the cell.

3.2. Electrochemical features and distribution of current field

Fig. 6 shows the anode, cathode electric potential, electrolyte potential distributions and the current direction in the electrolyte. Because the potential of the anode current collector is assumed to be zero, the electric potential in the porous anode is negative and gradually decreases from the current collector to the anode/electrolyte interface. Due to the high electric conductivity of the anode, the absolute value of electric potential is small. The electric potential in the porous cathode is a positive value and decreases from the cathode/electrolyte interface to the cathode current collector. Because the porous cathode is thin and its conductivity is relatively high, the variation of electric potential at cathode is very small. As shown in Fig. 6(c), the potential in electrolyte varies more significantly in the r-direction than in z-direction, and the current direction in the electrolyte is mainly vertical to the cathode/electrolyte interface. The reason is that the whole cathode is connected to the cathode current collector, and the potential difference between the electrolyte and cathode is much larger than that inside the electrolyte at z-direction.

Fig. 7 illustrates the distribution of electromotive force (Nernst potential) along z-direction. E_{Nernst} decreases along the flow direction because of the H_2 depletion and high water concentration. The EMF is about 30 mV less at the fuel outlet than at inlet, implying that the reduction of the reversible cell potential is one of the major reasons for the cell performance reduction. Because the change of O_2 molar fraction at porous cathode is relatively small, the primary effect to E_{Nernst} is H_2 molar fraction and H_2O molar fraction at anode/electrolyte interface. Comparing Fig. 4 with Fig. 7, the variation trend of E_{Nernst} is consistent with that of H_2 molar fraction.

Fig. 8 shows distribution of current density along the anode/electrolyte interface at z-direction. The current density along the cell z-direction is more uniform under the OC mode than under the other modes. The current density under the OC mode firstly decreases, reaches a minimum of 4200 A m^{-2} in the middle part of a 2 cm cell and then increases toward the fuel

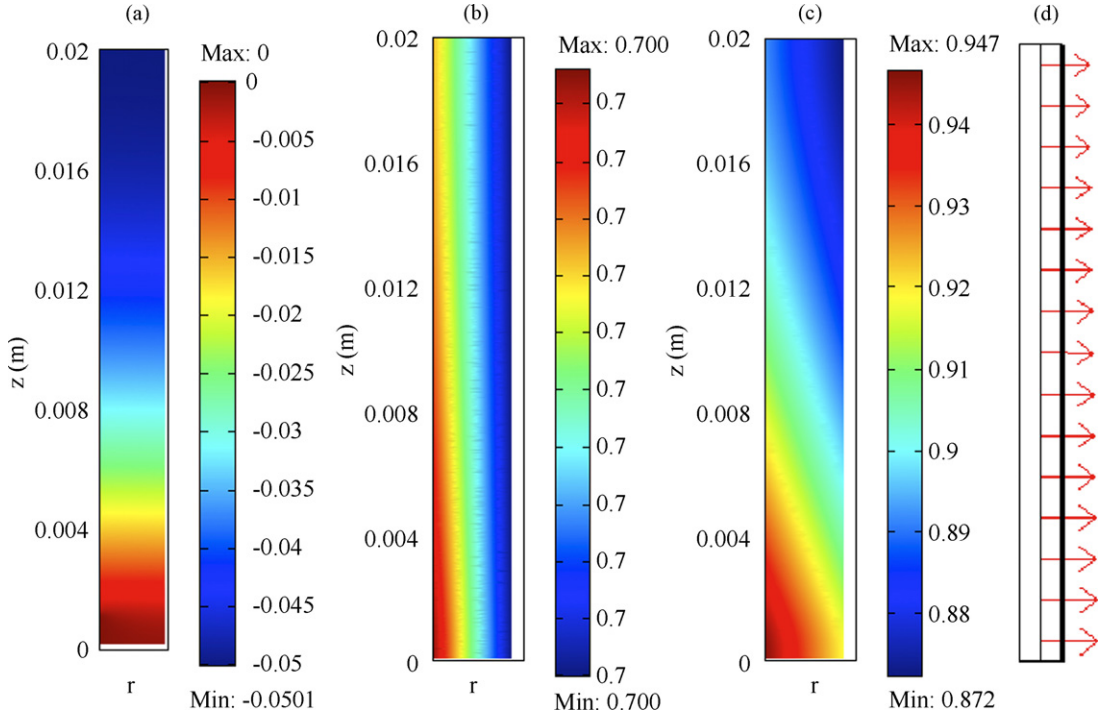

Fig. 6. Distributions of anode (a) and cathode (b) electric potentials, electrolyte (c) potential and the current direction (d) in the electrolyte.

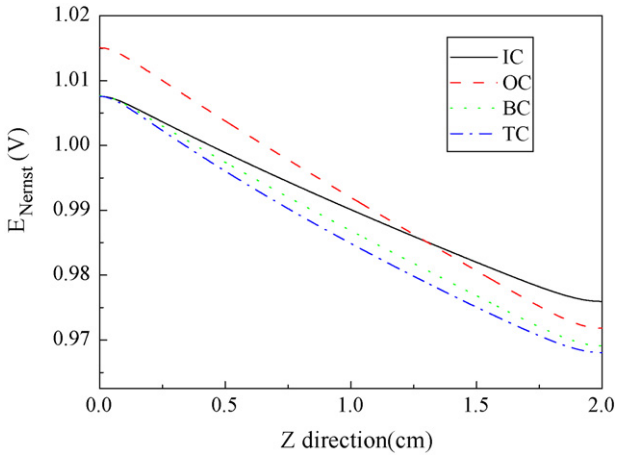

Fig. 7. Distribution of E_{Nernst} along the anode/electrolyte interface for a 2 cm long SOFC.

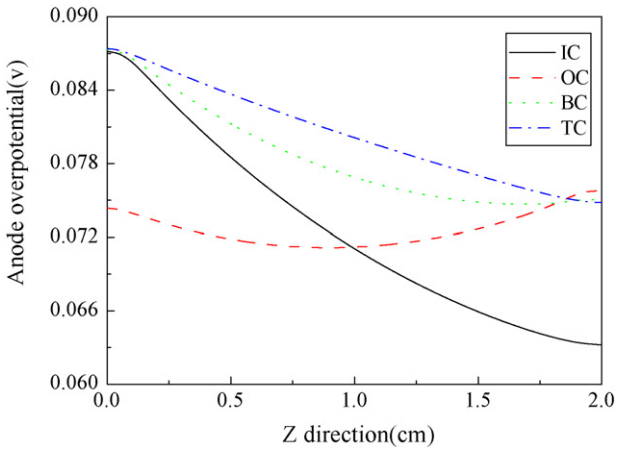

Fig. 9. Distribution of anode overpotential along the anode/electrolyte interface for a 2 cm long SOFC.

outlet. The difference between the maximum and minimum current densities is only 400 A m^{-2}, which is smallest among all these modes. The current density distribution is similar under the IC, BC and TC modes. For an example, the maximum of current density appears at inlet, and the minimum appears at outlet. Their current density at inlet under these modes are all close to 5700 A m^{-2}. The minimum current density under the BC and TC modes is 4900 A m^{-2} at the cell outlet, whereas the current density curve under the BC mode is concave because more energy is consumed by the longer current path. The current density under the IC mode at outlet is the smallest among all modes, and the difference of current density between inlet and outlet is 1500 A m^{-2}. Because the key parameters affecting the electrochemical reaction rate are the local H_2 and water concentrations, high H_2 concentration at the fuel inlet results in a high reaction rate. The current density under the OC mode keeps increasing when H_2 concentration decreases in the fuel outlet region because the influence of the current path on the current density is more severely than H_2 depleting rate. In a word, the electrochemical reaction under the OC mode is the most uniform one.

Fig. 9 and Fig. 10 show the distributions of anodic and cathodic overpotentials at electrode/electrolyte interfaces along the z-direction, respectively. The overpotential increases with current density increasing, vice versa. It is also seen that the cathodic overpotential is greater than the anodic overpotential in the cell because of inherently slower cathodic reaction kinetics [10].

Fig. 11 shows vector plots of current density inside anode and the effects of the four current collecting modes on the current path. The arrows express current-flow directions, and the arrow lengths are proportional to current density. Under the IC mode, current in anode flows from inlet to outlet and runs into cathode through the electrolyte, showing a gradually decreasing of current density in the outlet direction. Under the OC mode, current flow direction in anode is from outlet to inlet, and current density gradually decreases in current-flow direction. Under the BC mode, current in anode flows from both inlet and outlet to the tube center, and current density gradually decrease from the double ends to the tube middle. In this case, the current perpendicularly flows into the electrolyte in the tube middle. It can be seen that the longest current path under the BC mode is only

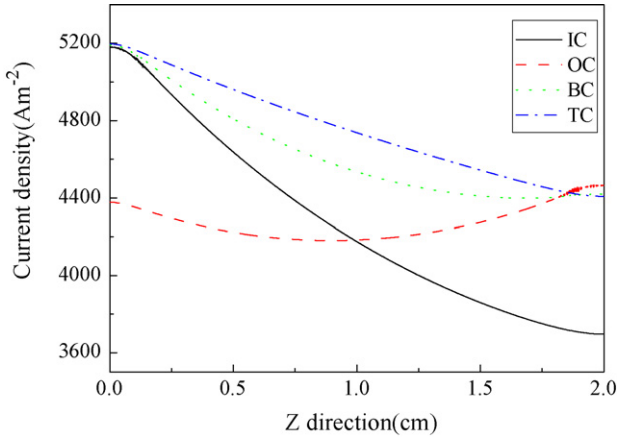

Fig. 8. Distribution of current density along the anode/electrolyte interface for a 2 cm long SOFC.

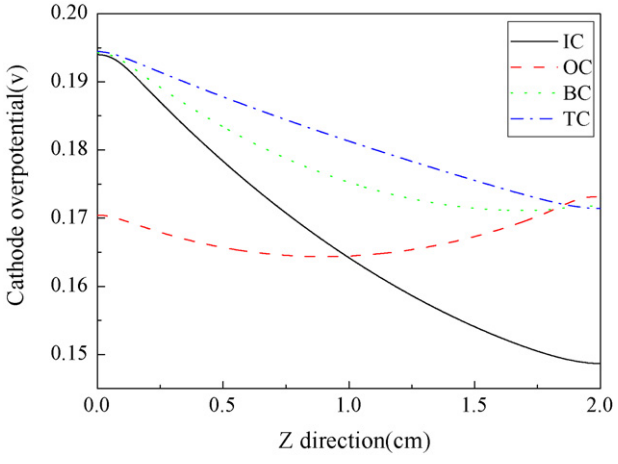

Fig. 10. Distribution of cathode overpotential along the anode/electrolyte interface for a 2 cm long SOFC.

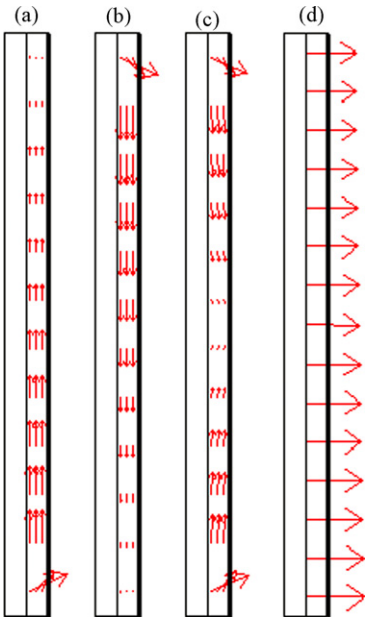

Fig. 11. Vector plots of current density inside anode under IC (a), OC (b), BC (c) and TC (d) modes.

half of that under the IC and OC modes. For the TC mode, the current-flow direction is perpendicular to the anode/electrolyte interface, and the current path is shortest among all modes. As far as the current collection is concerned, the TC mode gives the maximum efficiency. The efficiency and loss of the different current collecting modes are calculated by the following efficiency loss equations:

$$\text{efficiency} = \frac{I_i}{I_{TC}}. \tag{14}$$

$$\text{loss} = 1 - \frac{I_i}{I_{TC}}. \tag{15}$$

3.3. Effects of different current collecting modes

Fig. 12 shows the cell efficiency loss under the IC, OC and BC modes and the ratio of the IC loss over BC loss as a function of tube length for a 1.49 mm interior diameter micro-tubular SOFC at 800 °C. It can be seen that with the tube length increasing, the efficiency loss increases due to the increasing anode current path. It is shown that the cell efficiency loss is the same under the IC and OC modes but much smaller under the BC mode. For the different length anode, the efficiency loss is about 2–6-fold lower under the BC mode than under the IC and OC modes. Since the efficiency loss increases sharply when the anode length increases, the value of IC loss/BC loss decreases. It can be concluded that the BC mode is the most effective actual current collecting mode, under which the efficiency loss is less than 5% on a 2.5 cm long cell. It is shown that a shorter cell under the BC mode can effectively reduce the efficiency loss. The selection of the anode tube length and current collecting mode is very crucial to minimize the efficiency loss.

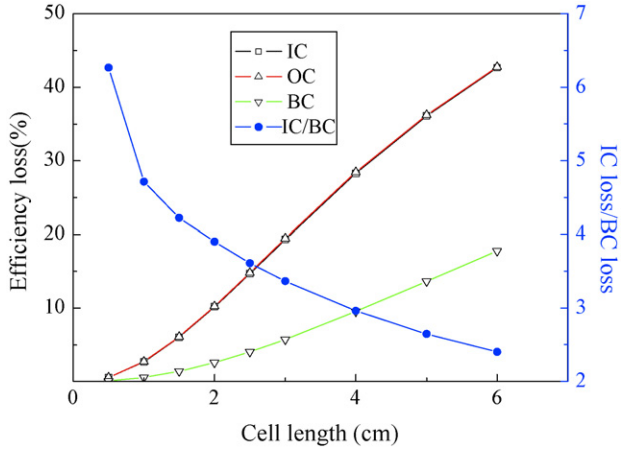

Fig. 12. The cell efficiency loss and IC loss/BC loss as a function of anode tube length.

4. Conclusions

In this paper, a 2D numerical analysis of the fluid dynamics and electrochemical kinetics has been conducted for anode-supported micro-tubular SOFCs. The variations of specie concentrations and electric potential in 2D have been obtained. The simulated current path inside the anode-supported micro-tubular SOFC could well reflect the current flow in an real cell. The current direction in electrolyte was mainly vertical to the cathode/electrolyte interface. The current flow in anode was mainly parallel to the anode/electrolyte interfaces and then flowed diagonally into the electrolyte. In addition, the cell geometry was also considered in the calculation of the cell performance. The current collecting efficiency was estimated with the simulation results of the cell under different current collection modes. The efficiency loss under the BC mode was about 2–6-fold lower than those obtained from the IC and OC modes, and the BC mode was the most effective current colleting mode. The anode current-collecting mode and tubular length were crucial for the design of micro-tubular SOFC. Those calculations using the model provided the optimum cell type and minimized efficiency loss.

Acknowledgements

The authors gratefully acknowledge financial supports from the Ministry of Science and Technology of China (No. 2004CB719506 and 2006AA05Z147) and Natural Science Foundation of China (No. 20676132).

References

[1] S.C. Singhal, K. Kendall, High Temperature Solid Oxide Fuel Cells: Fundamentals, Design and Applications, Elsevier, Kidlington, Oxford, 2003, p. 1.
[2] A. Yan, M. Cheng, Y. Dong, W. Yang, V. Maragou, S. Song, P. Tsiakaras, Appl. Catal. B 66 (2006) 64–71.
[3] H. Zhu, R.J. Kee, J. Power Sources 169 (2007) 315–326.
[4] Y. Du, N.M. Sammes, J. Power Sources 136 (2004) 66–71.
[5] J. Pusz, A. Smirnova, A. Mohammadi, N.M. Sammes, J. Power Sources 163 (2007) 900–906.
[6] N.M. Sammes, Y. Du, R. Bove, J. Power Sources 145 (2005) 428–434.

[7] H. Zhu, A.M. Colclasure, R.J. Kee, Y. Lin, S.A. Barnett, J. Power Sources 161 (2006) 413–419.
[8] T. Suzuki, T. Yamaguchi, Y. Fujishiro, M. Awano, J. Power Sources 163 (2006) 737–742.
[9] E. Achenbach, J. Power Sources 49 (1994) 333–348.
[10] M. Iwata, T. Hikosaka, M. Moriya, T. Iwanari, K. Ito, K. Onda, Y. Esaki, Y. Sakai, S. Nagata, Solid State Ionics 132 (2000) 297–308.
[11] H. Yakabe, T. Ogiwra, M. Hishinuma, I. Yasuda, J. Power Sources 102 (2001) 144–154.
[12] H. Yakabe, T. Sakurai, Solid State Ionics 174 (2004) 295–302.
[13] K.D. Panopoulos, L.E. Fryda, J. Karl, S. Poulou, E. Kakaras, J. Power Sources 159 (2006) 586–594.
[14] R. Bove, S. Ubertini, J. Power Sources 159 (2005) 543–559.
[15] S.H. Chan, K.A. Khor, Z.T. Xia, J. Power Sources 93 (2001) 130–140.
[16] P. Costamagna, A. Selimovic, M.B. Del, G. Agnew, Chem. Eng. J. 102 (2004) 61–69.
[17] C.-Y. Chung, Y.-C. Chung, J. Power Sources 154 (2005) 35–41.
[18] B.A. Haberman, J.B. Young, Int. J. Heat Mass Transf. 47 (2004) 3617–3629.
[19] Y. Ji, K. Yuan, J.N. Chung, Y.-C. Chen, J. Power Sources 161 (2006) 380–391.
[20] Y. Wang, F. Yoshiba, T. Watanabe, J. Power Sources 161 (2006) 380–391.
[21] B. Todd, J.B. Young, J. Power Sources 110 (2002) 186–200.
[22] R. Bove, P. Lunghia, N.M. Sammes, Int. J. Hydrogen Energy 30 (2005) 181–187.